Silicon Nanowire Polytypes: Identification by Raman Spectroscopy, Generation Mechanism, and Misfit Strain in Homostructures

Francisco J. Lopez,*,† Uri Givan,‡ Justin G. Connell,† and Lincoln J. Lauhon†,*

†Materials Science Department, Northwestern University, Evanston, Illinois. ‡Present address: Max Planck Institute for Microstructure Physics, Halle, Germany.

ABSTRACT

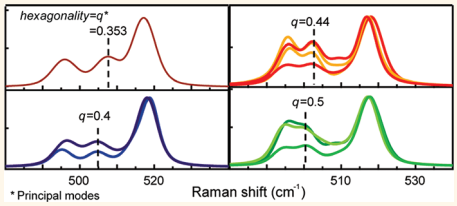

Silicon nanowires with predominant 9R, 27T, 2H and other polytype structures with respective hexagonalities of 50, 40 and 35.3% were identified by Raman microscopy. Transmission electron microscopy indicates that intrinsic stacking faults form the basic building blocks of these polytypes. We propose a generation mechanism in which polytypes are seeded from incoherent twin boundaries and associated partial dislocations. This mechanism explains observed prevalence of polytypes and trends in stacking for longer period structures. The percentage of hexagonal planes in a polytype is extracted from its Raman spectrum after correcting the zone-folded phonon frequencies to account for changes of the in-plane lattice parameter with respect to diamond cubic (3C) Si. The correction is found to be (i) of the same order of magnitude as frequency differences between modes of low period polytypes and (ii) proportional to the hexagonality. Corrected phonon frequencies agree with experimentally found values to within 0.4 cm^{-1}. Homostructures in which a central polytype region is bounded by 3C regions, with the planes $(111)_{3C} || (0001)_{polytype}$ parallel to the nanowire axis, are found in ⟨112⟩ oriented nanowires. Strain-induced shifts of the Raman modes in such structures enable a rough estimation of the lattice misfit between polytypes, which compares favorably with first-principles calculations. Considerations presented here provide a simple and quantitative framework to interpret Raman frequencies and extract crystallographic information on polytype structures.

KEYWORDS: silicon nanowire · polytype · Raman spectroscopy · grain boundary · homostructure

Crystal structure engineering in semiconductor nanowires has received increasing attention in the past few years with the demonstration of controlled twin superlattices and polytypes in III−V materials.[1−5] Several reports indicated the presence of hexagonal diamond stacking in silicon nanowires,[6−8] and conclusive evidence for the existence of ordered 2H and 9R polytypes in silicon nanowires was provided through high-resolution TEM images from a ⟨110⟩ zone axis and correlated Raman microscopy on individual nanowires.[9] In addition, single phase 2H Si was recently grown through epitaxy on wurtzite GaP nanowires.[10] The presence of the 9R polytype was also reported in macroporous silicon,[11] in which valence electron energy-loss spectra indicated a reduced *k* vector mismatch for optical transitions across the energy gap. Numerous theoretical calculations exist for the electronic band structure and corresponding optical and electronic properties of polytypes.[12−19] Whereas the localization of holes in 2H segments within 3C/2H superlattices is predicted by all calculations, the localization of electrons is not as clear, since the predicted conduction band offsets are small and sign changes are found between different calculations.[13,14,17] The possibility of type II band alignment would be of interest in light-absorbing devices due to extended carrier lifetimes. Measurements in silicon solar cells suggested longer carrier lifetimes on heavily twinned regions.[20] In addition, a reduced density of states effective mass for holes would result in greater mobilities for 2H.[19] Polytype homojunctions could add functionality to electronic and optoelectronic devices by exploiting band offsets, band splittings and modified energy gaps. For example, the expected decreasing energy gap with polytype hexagonality[12,18] and the resulting extension of light absorption into the near-infrared may also prove advantageous for solar energy applications based on these materials.[21] Here we report the stacking trends observed in a number of silicon polytypes, and discuss a mechanism for their formation as well as practical aspects of their identification by Raman microscopy.

* Address correspondence to francisco1591@gmail.com, lauhon@northwestern.edu.

Received for review August 16, 2011 and accepted October 21, 2011.

Published online October 21, 2011
10.1021/nn2031337

RAMAN FREQUENCIES OF FOLDED POLYTYPE MODES

Raman microscopy is a nondestructive and relatively high-throughput characterization technique compatible with *in situ* device measurements. Raman analysis can provide crystallographic information even without knowledge of nanowire orientation.[22] The throughput is particularly attractive for statistical analysis of the products of synthesis, Transmission Electron Microscopy (TEM) being relatively slow in comparison. In previous work, we showed that Raman microscopy could discriminate between disordered and ordered stacking sequences leading to new polytypes.[9] A zone-folding argument was used to qualitatively explain the appearance of additional modes in the spectrum.[23] A more thorough description of zone-folding is provided here as the foundation of quantitative analysis of peak frequencies from a variety of polytypic structures. The zone-folding argument is based on the fact that polytype phonon dispersions along the *c*-axis can be approximated from the dispersion of the cubic phase by folding the Brillouin zone *n* times along the $\Gamma \rightarrow L$ direction, with *1/n* being the reciprocal space period of a given polytype (relative to the period of 3C) .[23,24] Folding results in new optical phonon branches that satisfy the $q \approx 0$ selection rule for Raman scattering, leading to extra peaks on the spectrum. The number, frequency and relative intensities of these folded modes are characteristic of the stacking sequence of each polytype. For the 2H (9R) polytype, zone folding predicts TO folded modes of E_{2g} (E_g) symmetry corresponding to a reduced wavevector $q = 1$ ($q = 2/3$) in the unfolded cubic zone. These modes involve atom displacements parallel to the close-packed planes (planar modes). Additionally, A_{1g} (2H and 9R) modes vibrate parallel to the *c*-axis (axial modes) and have frequencies 4 or 5 cm^{-1} lower than the triply degenerate F_{2g} mode of cubic silicon. These mode assignments are consistent with polarization-dependent selection rules as well as first-principles calculation.[9,25]

Although in principle measuring the frequencies of first order Raman peaks is a straightforward means to identify polytypes, in practice, the quantitative interpretation of phonon frequencies requires additional analysis. As an initial challenge, the uncertainty in the phonon dispersion data $\omega_{3C}(q)$ from inelastic neutron scattering,[26,27] X-ray scattering[28] or theoretical calculations[29,30] is at best $\sim$2 cm^{-1}. This is larger than the frequency differences that are useful to measure for identification purposes, particularly considering that our Raman spectrometer can detect peak shifts of $\sim$0.1 cm^{-1} (even when the resolution is $\sim$1 cm^{-1}). The analysis below therefore utilizes the *shape* of the phonon dispersion calculated by first-principle methods,[29] while the location of zone center and boundary of the $\Gamma \rightarrow L$ TO branch are established by our experimental Raman data.

TABLE 1. Experimental frequencies of 2H and 9R compared to zone-folding predictions

Polytype	Folded *q* point	Planar modes (measured)	$\omega_{3C}(q)$ (from eq 1)	Axial modes (measured)
2H	2/2	495.6 +- 0.4	492	515.2 +- 0.8
9R	2/3	496.7 +- 0.3	494.3	515.8 +- 0.6

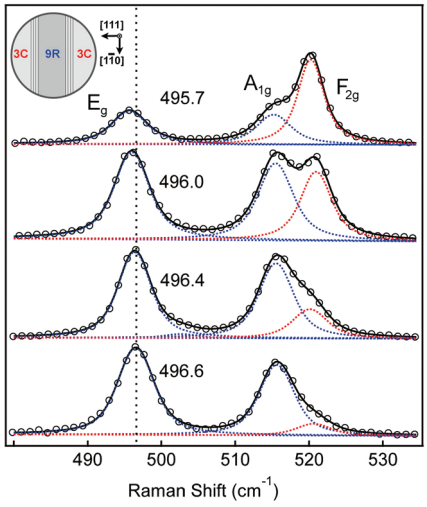

Figure 1. Raman spectra from four nanowires with different relative volumes of 9R (blue) and 3C (red) phases show a downshift of the E_g mode frequency of 9R with increasing amounts of 3C material. Schematic on top represents a cross-sectional view along the axis of a typical polytypic nanowire. Note $(111)_{3C} || (0001)_{9R}$.

The $\omega_{3C}(0)$ frequency of bulk Si in our system is 520.2 cm^{-1}, and the TO frequency at the *L* point $\omega_{3C}(1)$ was initially estimated from the position of the critical point associated with the 2TO(*L*) overtone in the Raman spectrum to be 491.5 $\pm$ 1 cm^{-1}. The experimental frequency span $\Delta\omega_{TO}(0) = \omega_{3C}(0) - \omega_{3C}(1)$ can then be used to calculate the dispersion

$$\omega_{3C}(q) = \omega_{3C}(1) + \Delta\omega_{TO} \cdot \hat{\omega}_{3C}(q) \qquad (1)$$

from a normalized dispersion $\hat{\omega}_{3C}(q)$ taken from a first-principles calculation.[29] We find that zone-folding predictions systematically underestimate experimental polytype frequencies and overestimate the frequency difference between the 2H and 9R folded modes (see Table 1). For example, the folded 2H mode should be equal to the TO $\omega_{3C}(L)$, but it is $\sim$3.6 cm^{-1} higher. We propose that this discrepancy can be explained by the nonideality of the *c*/*a* ratio of lattice constants of polytypes. We note that the values reported here are refined from our prior publication[9] as the identification of better specimens has enabled a more accurate estimation of the frequencies.

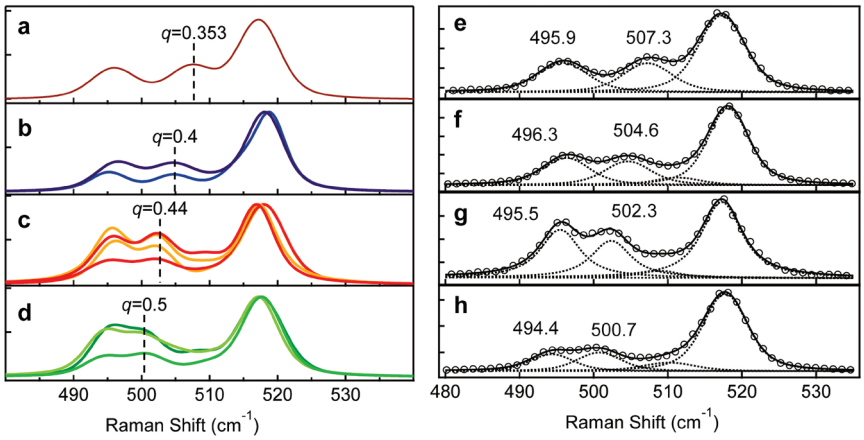

Figure 2. Fits to background subtracted Raman spectra are shown in (a)-(d) for four different polytypes whose principal folded modes ($q=h$) result from the indicated values of the reduced wavevectors q on the 3C phonon dispersion. The dashed lines in (a)-(d) indicate the frequencies of these q points calculated using eq 2. Spectra are consistent with (a) 51T, (b) 5H or 10H, (c) 27T and (d) 12R or 24T polytypes based on observed stacking trends. Corresponding fits of (solid line) and individual modes for (dashed line) spectra associated with each polytype (data in circles) are shown in (e)-(f), indicating the frequencies of the principal and lowest modes in each case.

Figure 1 shows spectra from nanowires with a 3C/9R/3C structure and varying amounts of the two phases. Cross-sectional TEM work confirmed the stacking faults extend through the entire nanowire cross section.[31] The frequency of the planar E_g mode of 9R increases continuously with decreasing intensity of the 3C modes. We attribute this shift to tensile strain within the (0009) planes of the 9R polytype imposed by the surrounding 3C material, which has a larger in-plane lattice constant. This is consistent with theoretical calculations for silicon and diamond[32,33] as well as recent experimental studies in III−V nanowires[34] which find that in-plane lattice constants decrease linearly with polytype hexagonality, while the average spacing between closed-packed planes increases. Besides introducing strain in polytype homostructures, changes in the lattice constants imply that a free-standing (strain-free) polytype will exhibit an increase in the frequency of the planar phonon modes and a reduction in the frequency of axial modes relative to the values expected from folding the 3C dispersion.

Assuming that the lattice constants of silicon polytypes vary linearly with the degree of hexagonality,[32−34] the frequency of any planar mode of a *pure* polytype can be calculated from its hexagonality h and reduced wavevector q in the unfolded zone as

$$\omega_{polytype}(q, h) = \omega_{3C}(q) + \alpha h \qquad (2)$$

where α is a constant given by the frequency difference $\omega_{2H}(1,1) - \omega_{3C}(1)$. This further assumes the correction αh is directly proportional to the change in lattice constant. The quantity defined as hexagonality gives the percentage of hexagonal planes (or density of twin planes in 3C) in a period of a polytype, and has long been used to correlate properties like lattice constants and energy band gaps of SiC.[23] From the experimental value for $\omega_{2H}(1,1)$ (Table 1), and eqs 1 and 2 we obtain $\alpha = 4.1 \pm 1.4\ cm^{-1}$, a value that we refine below.

IDENTIFICATION OF HEXAGONALITIES OF NEW SILICON POLYTYPES

We now compare experimentally measured frequencies with calculations from eq 2. In nanowires that exhibited at least two distinct folded modes of comparable intensity, spectra could be grouped into distinct classes (figure 2). Such nanowires were rare for our growth conditions, occurring in ~1% of the population with the exception of the type shown in figure 2c, which occurred with ~10% yield. Below we rely on the higher frequency folded mode for identification, since the lower modes more likely involve contributions from mixed phases, as evidenced by variations in relative intensities and frequencies. In addition, the axial polytype modes are generally not resolved from the cubic mode in these polytypes (with lower hexagonalities compared to 2H or 9R). Nakashima et al.[35] showed that the folded mode with strongest intensity is that for which $q = h$, which we refer to as the *principal* folded mode in the following analysis.

From eq 2 with $q = h$ we determine that the principal modes in figures 2b and 2d have frequencies corresponding to $q = 0.4$ and $q = 0.5$, respectively. Spectra in 2c exhibit a frequency midway between $q = 0.4$ and $q = 0.5$. The value $q = 4/9 = 0.44$ is the smallest denominator fraction that comes close to the observed wavenumber (within 0.4 cm^{-1}). The spectrum in 2a has a frequency between $q = 0.4$ and $q = 0.33$, and the values $q = 4/11$ and $q = 6/17$ are the smallest denominator fractions with an even numerator that come close to this. The requirement that the numerator be even follows directly from zone-folding. We choose 6/17 for having a calculated frequency greater than experiment; given the clean fit on 2e (only three peaks) we assume only

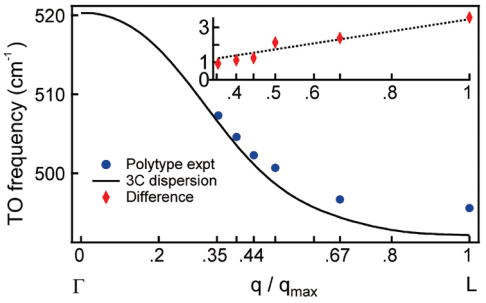

Figure 3. Comparison of the transverse optical phonon dispersion of 3C along [111] (black solid line) and frequencies of the principal folded modes for several silicon polytypes (blue circles). Deviations increase toward the zone boundary, and the difference (inset, red diamonds) is proportional to *q*. The frequencies of typical polytype inclusions in Si nanowires lie between the 3C dispersion frequency at the respective *q* and the calculated value for a pure polytype eq 2, which is close to the blue circles. The exact position depends on the relative content of 3C lateral bands, which impose tensile strain.

3C lateral bands may be present in addition to the main polytype, in which case we expect the experimental frequency to be somewhat lower than the calculated value (the lateral 3C bands impose tensile strain). The same assumption may not be made about spectrum in figure 2h, but the *q* assignment there is less ambiguous. After this preliminary assignment of the *q* values of these polytypes, we use eq 2 once more to arrive at a refined value for α by fitting data from figures 2e-h as well as data in Table 1 for 2H and 9R. This yields α = 3.6 ± 1 cm^{-1}. Calculated phonon frequencies for several polytypes are shown in the Supporting Information (Table S1). In figure 3 we compare the phonon dispersion of the cubic phase calculated as described before with experimentally observed principal mode polytype frequencies using our *q* assignments. It is seen that the difference between the folded polytype modes (blue circles) and the cubic dispersion (black line) is linear in *q*, indicating the assumptions made in eq 2 above hold to within uncertainties of about 0.4 cm^{-1}.

The spectra in figure 2 were acquired from nanowires dispersed on Au-coated silicon substrates, which precluded the acquisition of correlated TEM data. Although the phonon frequencies readily provide the hexagonality of the polytype, the detailed stacking sequence of longer period polytypes (as represented by Zhdanov symbol[36]) requires detailed analysis of the relative intensities of all folded modes, such as that carried out by Nakashima for SiC polytypes.[37,38] Such analysis is beyond the scope of this work. Nevertheless, specific stacking sequences observed in TEM images suggest that certain polytypes are favored. A brief explanation of polytype notation is useful for the discussion below.[36] The Ramsdell notation designates a polytype with two symbols *n*X, where *n* is the period of the polytype in a

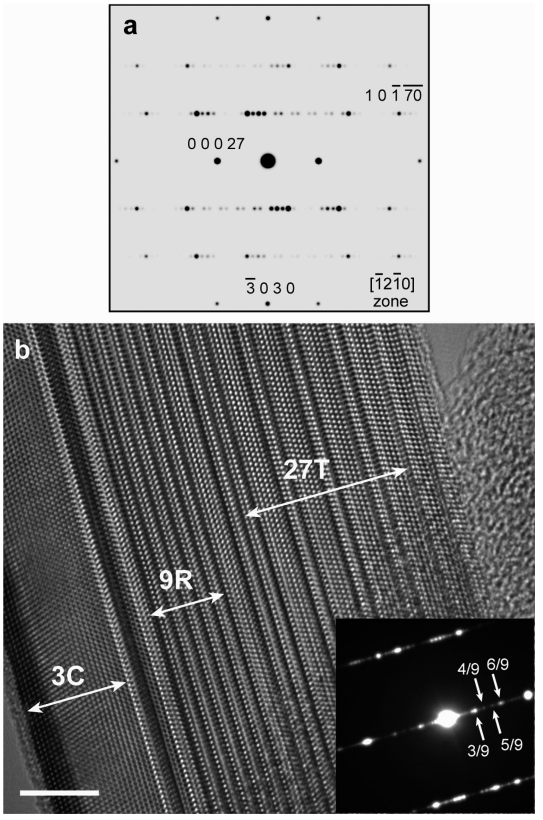

Figure 4. (a) Simulated kinematic electron diffraction pattern of a 27T Si structure show spots with 1/9 of the (111) spacing of 3C, corresponding to the 00027 reflection. (b) High resolution TEM image from a ⟨112⟩ oriented nanowire containing segments of 3C, 9R and 27T polytypes denoted with arrows. The Zhdanov sequence of the 27T polytype is $(2151)_3$, where alternating twin domains with different orientation appear successively in bright and dark contrast; a total of 36 bilayers are present with uninterrupted 27T stacking. Between the 9R and 27T polytypes, the sequence 2141 is observed. (inset) Selected area electron diffraction pattern shows weak spots with 1/9(111) spacing characteristic of 27T as well as stronger 1/3(111) spots characteristic of both 9R and 27T. Scale bar is 5 nm.

hexagonal unit cell and X denotes the lattice type, which can be hexagonal (H), rhombohedral (R), trigonal (T) or in one special case cubic (C). The Zhdanov notation assigns a sign to each bilayer depending on the orientation of the next bilayer: (+) for layers in the normal orientation (A→B→C→A) and (-) for twinned layers (A→C→B→A). Each number in the Zhdanov symbol denotes the number of consecutive layers with the same sign. 3C, 2H and 9R are represented as (∞), (11) and $(21)_3$, respectively. The sequence repeats three times for trigonal and rhombohedral polytypes, which is indicated by the subscript 3, although it is often omitted for rhombohedral lattices. The Zhdanov notation is the most compact symbol that fully represents the stacking sequence, and the contrast in a HRTEM image from an equivalent ⟨2$\bar{1}\bar{1}$0⟩ zone may be directly correlated with sign of the bilayers for slight off-zone misorientation (*c*-axis off the plane normal to the beam).[39]

Figure 4 shows TEM imaging and electron diffraction from a nanowire that has distinct segments with 3C, 9R and 27T stacking. The Zhdanov sequence for the 27T segment is $(2151)_3$. Selected-area diffraction shows weak spots with 1/9(111) spacing characteristic of 27T in addition to stronger spots with 1/3(111) spacing characteristic of both 9R and 27T. The 27T structure belongs to the space group *P*3m1 (156) of the trigonal system, and its simulated kinematical electron diffraction pattern is shown in Figure 4a, where characteristic 1/9(111) spots can be seen. A nanowire specimen with this structure was identified as *cccchhchh* (in the Jagodzinski notation) in a recent report,[40] which is equivalent to the Zhdanov symbol $(2151)_3$. The Jagodzinski notation[36] assigns letters *c* (cubic) or *h* (hexagonal) to each bilayer depending on whether the two neighboring bilayers occupy different or equal sites (A,B or C), respectively. A 27R structure was also reported in silicon whiskers,[41] although the stacking sequence was not indicated and a rhombohedral lattice was assumed. Interestingly, this early work reported that the `overwhelming majority' of whiskers had a 6H structure, suggesting the possibility of obtaining significantly higher polytype yields than we have obtained in this work (we observe 9R most abundantly, but with yields of 20 to 30%). Miyamoto et al.[41] also reported the observation of the 51R polytype, which has $h = 6/17$, although they did not report on the detailed stacking sequence. This structure is consistent with the Raman spectrum in figure 2a. Note that the hexagonality of a polytype is obtained directly as the ratio of number of digits divided by their sum from the Zhdanov sequence.

TRENDS IN STACKING SEQUENCE AND STRUCTURAL ORIGINS

We note that 2H, 9R and 27T polytypes can be described as a periodic array of intrinsic stacking faults (ISF), with one of the twin orientations always appearing with only one bilayer (the `1's in the Zhdanov sequence). The stacking sequence for 9R is AB|C|BC|A|CA|B|, where each twin domain is separated by a vertical bar. Twin planes appear in pairs, leading to a missing plane of atoms every 3 bilayers as compared to 3C stacking. The value $h = 2/3$ follows from the density of twins. The sequence for 27T polytype with Zhdanov symbol $(2151)_3$ is AB|C|BCABC|A|CA|B|ABCAB|C|BC|A|CABCA|B|, hence $h = 4/9$. This structure is likely responsible for the Raman spectra in figure 2c. One would not necessarily expect that ISFs are prevalent planar defects in silicon nanowires given their higher formation energy compared to single twins or extrinsic stacking faults.[14] The prevalence of ISFs suggests seeding from other defects as the structural origin of the observed long-period polytypes. Specifically, it has been demonstrated that an incoherent ⟨110⟩ Σ3 (112) symmetric tilt boundary reconstructs giving rise to a 9R polytype band in fcc metals.[42,43] In this case, grain boundary dislocations dissociate into partials forming an array of ISFs, giving rise to the narrow polytype band. The phenomenon appears to be quite general for symmetric ⟨110⟩ tilt boundaries for some ranges of the misorientation angle, as long as the stacking fault energy is low so that dissociation is energetically favorable.[44,45] An asymmetric 90° {111}/{112} boundary has also been reported to dissociate forming a 9R band at the interface.[46] It has been shown that 2H forms from dissociation of a {533} Σ43 symmetric boundary in gold,[47] where the grain boundary was related to the periodicity of ISFs by geometric considerations. Other polytypes could result from deviations of the low energy misorientation angles; boundaries with arbitrary angle may decompose into energetically more favorable units introducing secondary dislocations.[44] In the case of silicon, both experiments[48] and molecular dynamics simulations[20] of growth on ⟨110⟩ tilt grain boundaries lead to the nucleation of stacking faults that propagate through subsequent growth stages. We hypothesize that at high droplet supersaturations, atypical nucleation events can lead to the formation of incoherent grain boundaries in Si nanowires. Coherent Σ3 twin formation has been associated with kinking from a ⟨111⟩ to ⟨112⟩ growth direction at sufficiently high supersaturations[49] and modifications of the droplet energetics associated with the kinking may also play a role in the generation of ordered planar defects. It remains unclear however, how layer by layer nucleation may spontaneously generate ordered ISF arrays with long repeat units in the absence of a seeding mechanism.

While the structure that Miyamoto et al. identified as 6H (33) does not follow the stacking trends we describe here, the evidence that they provided for 6H is consistent with an 18R structure as well. The 18R structure with sequence $(51)_3$ appears to be a more likely candidate, since it is a building block for the relatively abundant 27T polytype (figure 4), that can be described as the superstructure $(9R)_1(18R)_1$. Trends in the periodicities of grain boundary dislocation arrays can also result from association of short period structures that repeat to form superstructures with longer periods.[50] We conclude from these observations that the proposed mechanism for seeding of polytypes from grain boundary dislocations, while speculative, accounts for the observed prevalence of ISFs, trends in stacking of longer period polytypes, as well as typical features observed in 3C/polytype/3C nanowire structures. Further electron microscopy studies are required to reveal the detailed geometry of the twin crystals and boundaries involved in order to describe a detailed growth mechanism.

Considering the observed trends in stacking, we discuss possible stacking sequences associated with the spectra in figure 2. Although 4H is the simplest structure that could give rise to Raman spectra in figure

2d, it does not follow from a periodic array of ISF. Extrinsic stacking faults were rarely observed for our growth conditions, but we note that 4H has been reported in low-pressure chemical vapor deposition of polycrystalline silicon.[51] In our nanowires, other structures like $(31)_3$, $(2141)_3$ and $(1151)_3$ seem more likely . Of these, we have observed the last two on the TEM, and the sequence 2141 can be found between the 9R and 27T inclusions in the nanowire in figure 4. By the same arguments, spectra in figure 2b could result from the 41 sequence corresponding to 5H with $h = 2/5$ or from the 2161 sequence, a 10H polytype with $h = 4/10$. 5H is perhaps more likely given that it is a building block of the $(2141)_3$ polytype, which can be described as $(9R)_1(5H)_1$. Numerous sequences[52] are possible for the spectrum in figure 2a, including $(515141)_3$ and $(216161)_3$ both with $h = 6/17$. The former sequence can be described as $(18R)_2(5H)_1$.

LATTICE CONSTANT VARIATION WITH HEXAGONALITY

The identification of relatively pure 3C/9R/3C structures with varying amounts of the 9R polytype (as in figure 1) enables examination of the dependence of peak frequencies on the fractional intensity of the 9R modes $I_{9R}/[I_{9R} + I_{3C}]$. This ratio approximates the actual volume fraction x of the 9R phase (see detailed discussion in Supporting Information). The peak shifts $\Delta\omega$ are linear for small strains,[53] so for a 9R mode in such structure we have

$$\Delta\omega_{9R}(x) \equiv \omega_{9R}(x) - \omega_{9R}(1) \cong k \cdot f_{9R}(1 - x) \qquad (3)$$

where k is the strain-induced peak shift coefficient and f_{9R} is the misfit of the in-plane lattice parameter of 9R relative to 3C. Knowledge of k allows one to estimate f_{9R} and thus the in-plane lattice constant of 9R.

Figure 5 shows the dependence of the frequencies of 9R and 3C modes on the fraction of 9R intensity. Remarkably, the magnitude of the shift is approximately linear, and the fitted slope gives $-\Delta\omega_{9R}(x \to 0)$. The trend is especially clear for the E_g mode of 9R, with a shift of -2.3 cm^{-1}. This value can be compared with the difference obtained from eq 2: $\omega_{3C}(q = 2/3) - \omega_{9R}(q = 2/3) = -2\alpha/3 = -2.4$ cm^{-1}. This second frequency shift results from modeling the change in lattice constants between 3C and 9R as a (111) biaxial compression of 3C. That is, the 3C doublet mode under compressive strain would shift by the same amount as the 9R planar mode under pure biaxial tension resulting from lattice misfit, suggesting that biaxial compression of 3C is a good approximation for modeling the shift of polytype frequencies. This approximation becomes necessary in the absence of measured experimental values of k for polytypes. With regards to the validity of the approximation, we note that Sui and Herman[54] investigated theoretically the evolution of 3C phonon frequencies of the entire TO branch along

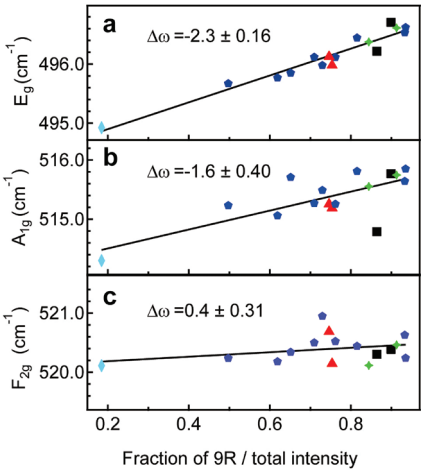

Figure 5. Dependence of the Raman frequency of (a)-(b) 9R and (c) 3C modes on the fraction of intensity from the 9R modes in 3C/9R structures. Symbols denote nominal diameters of the catalyst gold nanoparticles used to grow the nanowires: 30 nm (triangles), 40 nm (squares), 50 nm (pentagons), 80 nm (stars) and 100 nm (diamond). Frequencies increase proportional to the amount of 9R, without showing systematic dependence on the diameters. Frequency shifts $\Delta\omega$ relative to free-standing unstrained materials were determined by extrapolating a linear fit to the end points 0 and 1, corresponding to fully strained (3C in-plane lattice constant) and unstrained material, respectively.

$\Gamma \to L$ under a (111) biaxial strain of 4% (Si on Ge). They found the shift was nearly independent of q with a maximum deviation of 10% at the zone boundary. Additionally, theoretical calculations of the elastic constants of 2H,[55] deviate less than 5% from what would be expected from a geometrical transformation of the cubic constants[22] with the exception of C_{44} deviating by 21%. These studies further support the value of k from 3C is a reasonable approximation for the corresponding polytype coefficients. From reported values for the Raman shift coefficient $k_d = -1053\ cm^{-1}$ of the doublet mode for biaxial strain on (111) 3C[56] and our value for $\alpha = 3.6\ cm^{-1}$ we estimate the misfit f_{2H} between 2H and 3C:

$$f_{2H} = -\alpha/k_d = 0.0034 \pm 0.001$$

which gives $\alpha = 3.827$ Å for the in-plane lattice constant of 2H. This reduction from the 3C value agrees with $f_{2H} = 0.0033$ calculated by first-principles.[57] Note that k_d is relatively large, indicating that in principle, Raman spectroscopy can detect strains on the order 0.01% (a shift of ~0.1 cm^{-1}) in this geometry. Previous experimental reports of the 2H lattice constant range between $\alpha = 3.80$ to 3.86 Å(see[10,32] and references therein). The Raman-based methodology is useful in view of the difficulty of performing X-ray diffraction on individual nanowires and the fact that typical uncertainties in TEM measurements (1 or 2%) are larger than the lattice misfit between 3C and polytypes. Since Raman spectroscopy probes strain directly, uncertainties in the estimated

lattice constants remain small even if the strain estimate is off as much as 30%, because the misfit between polytypes is a small quantity. For a detailed discussion of approximations made in this estimation, as well as discussion of the effect of phonon confinement on the measured Raman frequencies, see the Supporting Information. Finally we note that a biaxial strain, as discussed above for polytype homostructures, could be desirable for higher electron mobilities. For the case of 2H such a strain is expected to split the three equivalent conduction-band minima located at M in the Brillouin zone, resulting in lower density of states electron effective mass.[19]

In summary, silicon nanowires with a variety of polytype structures were observed. A generation mechanism was proposed in which nanowire polytypes are seeded from grain boundary dislocation arrays. Raman frequencies of polytypes were calculated and found to be accurate experimentally to within 0.4 cm^{-1}. Observed Raman frequencies in polytype homostructures are consistent with an in-plane lattice constant that decreases linearly with hexagonality, with the largest misfit of 0.34 $\pm$ 0.1% between 2H and 3C polytypes. Homostructures of 3C/2H/3C and other polytypes may find applications exploiting their coherent interfaces and expected distinct optical and electronic properties.

METHODS

Nanowires were grown in a 1-in. quartz tube furnace from colloidal Au catalyst particles dispersed on Si substrates. The growth was carried out at a total pressure of 40 Torr with 20 sccm of H_2 and 30 sccm of He gas as carriers. The silane flow was varied between 2 and 6 sccm. Growths were carried out at temperatures in the range 430 - 470 °C. Detailed analysis of the polytype yield for different growth conditions is beyond the scope of this work.

TEM measurements were described previously.[9] In all Raman measurements, a confocal microscope (Witec) with 532 nm laser focused with a 0.9 numerical aperture and 100x objective (spot size about 0.7 μm) was used to excite scattering, with both incident and scattered polarization parallel to the nanowire axis. Excitation powers ranged between 10 and 100 μW; corresponding integration times varied between 100 and 300 s for final spectrum acquisition and 1 to 5 s for initial survey spectra, as we browsed through many nanowires. To ensure that laser-induced heating did not affect the measured peak frequencies, the power was lowered until no peak shift was observed upon further power reduction. The method is valid so long as the signal-to-noise ratio from the spectrum is sufficient to detect the peak shift. The microscope used a triple axis piezoelectric motion stage which allowed precise positioning of the sample, important to maximize Raman signal collection. The nanowires investigated had Raman spectra that did not change significantly along the axial length and had diameters between 30 and 100 nm. Scattered light was not analyzed for nanowires with diameters <50 nm, since light polarized perpendicular to the nanowire contributed less than ~5% to the total intensity. Backscattered light was collected through the same objective and subsequently coupled into an optical fiber connecting the microscope and the spectrometer. The diameter of the fiber acted as an entrance slit for the spectrometer, controlling spectral resolution at the expense of signal throughput. Spectra were acquired with a 50 μm diameter fiber core. All spectra were fit with Voigt line profiles. Correlated TEM and Raman studies were performed on individual nanowires by dispersing from an ultrasonicated suspension onto lacey carbon Cu grids, though most of the Raman data presented here were acquired from nanowires dispersed on Au coated (80 nm) Si (100) substrates (without TEM data). The gold film blocked the Raman signal from the underlying Si substrate and provided a thermal sink to minimize laser beam induced heating of the nanowires, which was comparatively high for freely suspended nanowires. In silicon, the frequency separation of the strongest modes of several low period polytypes is only about 1 or 2 cm^{-1}. It is therefore important to investigate straight nanowires to avoid any strain induced shifts.[58] Similarly, diameters smaller than about 30 nm (nominal size of catalyst seed) were avoided to prevent the long integration times required to obtain good quality spectra and to simplify line shape analysis as determined by crystal structure, avoiding phonon confinement effects.[59] The spectrometer was calibrated using a mercury−argon lamp, and in each session we measured the line of a bulk crystalline silicon substrate, assumed to be the reference for 520.2 cm^{-1}, for possible minor deviations from the alignment.

Acknowledgment. F.J.L. and L.J.L designed the study. F.J.L analyzed and interpreted the Raman and TEM data. F.J.L. and U.G. chose polytype nanowire growth conditions and U.G. and J.C. carried out the growths. F.J.L. wrote the manuscript and L.J.L. reviewed and edited. This work was supported by the Department of Energy Office of Basic Energy Sciences DE-FG02-07ER46401. F.J.L. acknowledges partial support from the National Council for Science and Technology (Mexico). L.J.L acknowledges the support of the Camille and Henry Dreyfus Foundation. We acknowledge the Northwestern University Atomic and Nanoscale Characterization Center for the use of the microscopy facilities. We acknowledge Eric Hemesath for the TEM image.

Supporting Information Available: Table of calculated Raman frequencies of polytypes, comments on phonon confinement and estimations of polytype volume fractions. This material is available free of charge *via* the Internet at http://pubs.acs.org

REFERENCES AND NOTES

1. Algra, R. E.; Verheijen, M. A.; Borgstrom, M. T.; Feiner, L. F.; Immink, G.; van Enckevort, W. J. P.; Vlieg, E.; Bakkers, E. P. A. M. Twinning Superlattices in Indium Phosphide Nanowires. *Nature* **2008**, *456*, 369–372.

2. Caroff, P.; Dick, K. A.; Johansson, J.; Messing, M. E.; Deppert, K.; Samuelson, L. Controlled Polytypic and Twin-Plane Superlattices in III-V Nanowires. *Nature Nanotechnol.* **2009**, *4*, 50–55.
3. Dick, K. A.; Caroff, P.; Bolinsson, J.; Messing, M. E.; Johansson, J.; Deppert, K.; Wallenberg, L. R.; Samuelson, L. Control of III-V Nanowire Crystal Structure by Growth Parameter Tuning. *Semicond. Sci. Technol.* **2010**, *25*, 024009.
4. Dick, K. A.; Thelander, C.; Samuelson, L.; Caroff, P. Crystal Phase Engineering in Single InAs Nanowires. *Nano Lett* **2010**, *10*, 3494–3499.
5. Joyce, H. J.; Wong-Leung, J.; Gao, Q.; Tan, H. H.; Jagadish, C. Phase Perfection in Zinc Blende and Wurtzite III-V Nanowires Using Basic Growth Parameters. *Nano Lett* **2010**, *10*, 908–915.
6. Cao, L. Y.; Laim, L.; Ni, C. Y.; Nabet, B.; Spanier, J. E. Diamond-Hexagonal Semiconductor Nanocones with Controllable Apex Angle. *J. Am. Chem. Soc.* **2005**, *127*, 13782–13783.
7. Morral, A. F. I.; Arbiol, J.; Prades, J. D.; Cirera, A.; Morante, J. R. Synthesis of Silicon Nanowires with Wurtzite Crystalline Structure by Using Standard Chemical Vapor Deposition. *Adv. Mater.* **2007**, *19*, 1347–1351.
8. Liu, X. H.; Wang, D. W. Kinetically-Induced Hexagonality in Chemically Grown Silicon Nanowires. *Nano Research* **2009**, *2*, 575–582.
9. Lopez, F. J.; Hemesath, E. R.; Lauhon, L. J. Ordered Stacking Fault Arrays in Silicon Nanowires. *Nano Lett* **2009**, *9*, 2774–2779.
10. Algra, R. E.; Hocevar, M.; Verheijen, M. A.; Zardo, I.; Immink, G. G. W.; van Enckevort, W. J. P.; Abstreiter, G.; Kouwenhoven, L. P.; Vlieg, E.; Bakkers, E. P. A. M. Crystal Structure Transfer in Core/Shell Nanowires. *Nano Lett* **2011**, *11*, 1690–1694.
11. Gu, L.; Yu, Y.; Sigle, W.; Usami, N.; Tsukimoto, S.; Maier, J.; Ikuhara, Y.; van Aken, P. A. Direct Bandgap Measurements in a Three-Dimensionally Macroporous Silicon 9R Polytype Using Monochromated Transmission Electron Microscope. *Appl. Phys. Lett.* **2010**, *97*, 213102.
12. Murayama, M.; Nakayama, T. Electronic-Structures of Hetero-Crystalline Semiconductor Superlattices. *J. Phys. Soc. Jpn.* **1992**, *61*, 2419–2433.
13. Murayama, M.; Nakayama, T. Chemical Trend of Band Offsets at Wurtzite Zincblende Heterocrystalline Semiconductor Interfaces. *Phys Rev B* **1994**, *49*, 4710–4724.
14. Chou, M. Y.; Cohen, M. L.; Louie, S. G. Theoretical-Study of Stacking-Faults in Silicon. *Phys Rev B* **1985**, *32*, 7979–7987.
15. Ikonic, Z.; Srivastava, G. P.; Inkson, J. C. Optical-Properties of Twinning Superlattices in Diamond-Type and Zincblende-Type Semiconductors. *Phys Rev B* **1995**, *52*, 14078–14085.
16. Persson, C.; Janzen, E. Electronic Band Structure in Hexagonal Close-Packed Si Polytypes. *J Phys-Condens Mat* **1998**, *10*, 10549–10555.
17. Raffy, C.; Furthmuller, J.; Wagner, J. M.; Bechstedt, F. Ab Initio Study of Structural and Electronic Properties of Planar Defects in Si and SiC. *Phys Rev B* **2004**, *70*, 195344.
18. Nakamura, J.; Natori, A. Dielectric Discontinuity at Structural Boundaries in Si. *Appl. Phys. Lett.* **2006**, *89*, 053118.
19. Malone, B. D.; Sau, J. D.; Cohen, M. L. Ab Initio Survey of the Electronic Structure of Tetrahedrally Bonded Phases of Silicon. *Phys Rev B* **2008**, *78*, 035210.
20. Pohl, J.; Muller, M.; Seidl, A.; Albe, K. Formation of Parallel (111) Twin Boundaries in Silicon Growth from the Melt Explained by Molecular Dynamics Simulations. *J. Cryst. Growth* **2010**, *312*, 1411–1415.
21. Boettcher, S. W.; Spurgeon, J. M.; Putnam, M. C.; Warren, E. L.; Turner-Evans, D. B.; Kelzenberg, M. D.; Maiolo, J. R.; Atwater, H. A.; Lewis, N. S. Energy-Conversion Properties of Vapor-Liquid-Solid-Grown Silicon Wire-Array Photocathodes. *Science* **2010**, *327*, 185–187.
22. Kim, K.; Lambrecht, W. R. L.; Segall, B. Elastic Constants and Related Properties of Tetrahedrally Bonded BN, AlN, GaN, and InN. *Phys Rev B* **1996**, *53*, 16310–16326.
23. Feldman, D. W.; Parker, J. H.; Choyke, W. J.; Patrick, L. Phonon Dispersion Curves by Raman Scattering in Sic Polytypes 3c,4h,6h,15r,and 21r. *Phys. Rev.* **1968**, *173*, 787–793.
24. Nakashima, S.; Harima, H. Raman Investigation of SiC Polytypes. *Phys Status Solidi A* **1997**, *162*, 39–64.
25. Wu, B. R. First-Principles Study on the High-Pressure Behavior of the Zone-Center Modes of Lonsdaleite Silicon. *Phys Rev B* **2000**, *61*, 5–8.
26. Nilsson, G.; Nelin, G. Study of Homology between Silicon and Germanium by Thermal-Neutron Spectrometry. *Phys Rev B* **1972**, *6*, 3777.
27. Kulda, J.; Strauch, D.; Pavone, P.; Ishii, Y. Inelastic-Neutron-Scattering Study of Phonon Eigenvectors and Frequencies in Si. *Phys Rev B* **1994**, *50*, 13347–13354.
28. Burkel, E. Phonon Spectroscopy by Inelastic X-ray Scattering. *Rep. Prog. Phys.* **2000**, *63*, 171–232.
29. Giannozzi, P.; Degironcoli, S.; Pavone, P.; Baroni, S. Ab Initio Calculation of Phonon Dispersions in Semiconductors. *Phys Rev B* **1991**, *43*, 7231–7242.
30. Savrasov, S. Y. Linear-Response Theory and Lattice Dynamics: A Muffin-Tin-Orbital Approach. *Phys Rev B* **1996**, *54*, 16470–16486.
31. Hemesath, E. R. Electron Microscopy Studies of Defect Structure and Correlated Impurity Incorporation in Si and Ge Nanowires. PhD Thesis. Northwestern University, 2010.
32. Raffy, C.; Furthmuller, J.; Bechstedt, F. Properties of Hexagonal Polytypes of Group-IV Elements from First-Principles Calculations. *Phys Rev B* **2002**, *66*, 075201.
33. Wen, B.; Zhao, J. J.; Bucknum, M. J.; Yao, P. K.; Li, T. J. First-Principles Studies of Diamond Polytypes. *Diamond Relat. Mater.* **2008**, *17*, 356–364.
34. Kriegner, D.; Panse, C.; Mandl, B.; Dick, K. A.; Keplinger, M.; Persson, J. M.; Caroff, P.; Ercolani, D.; Sorba, L.; Bechstedt, F.; Stangl, J.; Bauer, G. Unit Cell Structure of Crystal Polytypes in InAs and InSb Nanowires. *Nano Lett* **2011**, *11*, 1483–1489.
35. Nakashima, S.; Hangyo, M. Raman Intensity Profiles and the Stacking Structure in SiC Polytypes. *Solid State Commun.* **1991**, *80*, 21–24.
36. Durovic, S.; Krishna, P.; Pandey, D. Notations for Close-Packed Structures. *International Tables for Crystallography* **2006**, *C*, 752–753.
37. Nakashima, S.; Tahara, K. Raman-Scattering Determination of Structures for Sic Polytypes - Quantitative-Evaluation with a Revised Model of Lattice-Dynamics. *Phys Rev B* **1989**, *40*, 6339–6344.
38. Nakashima, S.; Kisoda, K.; Gauthier, J. P. Raman Determination of Structures of Long-Period Sic Polytypes. *J. Appl. Phys.* **1994**, *75*, 5354–5360.
39. Pirouz, P.; Chaim, R.; Dahmen, U.; Westmacott, K. H. The Martensitic-Transformation in Silicon 0.1. Experimental-Observations. *Acta Metall. Mater.* **1990**, *38*, 313–322.
40. Su, Z. X.; Dickinson, C.; Wan, Y. T.; Wang, Z. L.; Wang, Y. W.; Sha, J. A.; Zhou, W. Z. Crystal Growth of Si Nanowires and Formation of Longitudinal Planar Defects. *Crystengcomm* **2010**, *12*, 2793–2798.
41. Miyamoto, Y.; Hirata, M. Polytypism and Amorphousness in Silicon Whiskers. *J. Phys. Soc. Jpn.* **1978**, *44*, 181–190.
42. Ernst, F.; Finnis, M. W.; Hofmann, D.; Muschik, T.; Schonberger, U.; Wolf, U.; Methfessel, M. Theoretical Prediction and Direct Observation of the 9R Structure in Ag. *Phys. Rev. Lett.* **1992**, *69*, 620–623.
43. Wolf, U.; Ernst, F.; Muschik, T.; Finnis, M. W.; Fischmeister, H. F. The Influence of Grain-Boundary Inclination on the Structure and Energy of Sigma=3 Grain-Boundaries in Copper. *Philos Mag A* **1992**, *66*, 991–1016.
44. Rittner, J. D.; Seidman, D. N. <110> Symmetric Tilt Grain-Boundary Structures in fcc Metals with Low Stacking-Fault Energies. *Phys Rev B* **1996**, *54*, 6999–7015.
45. Rittner, J. D.; Seidman, D. N.; Merkle, K. L. Grain-Boundary Dissociation by the Emission of Stacking Faults. *Phys Rev B* **1996**, *54*, 5179–5180.
46. Medlin, D. L.; Foiles, S. M.; Cohen, D. A Dislocation-Based Description of Grain Boundary Dissociation: Application to a 90 degrees <110 > Tilt Boundary in Gold. *Acta Mater* **2001**, *49*, 3689–3697.

47. Medlin, D. L.; Lucadamo, G. Geometric Origin of Hexagonal Close Packing at a Grain Boundary in Gold. *Science* **2003**, *300*, 1272–1275.
48. Kitamura, M.; Usami, N.; Sugawara, T.; Kutsukake, K.; Fujiwara, K.; Nose, Y.; Shishido, T.; Nakajima, K. Growth of multicrystalline Si with controlled grain boundary configuration by the floating zone technique. *J. Cryst. Growth* **2005**, *280*, 419–424.
49. Dayeh, S. A.; Wang, J.; Li, N.; Huang, J. Y.; Gin, A. V.; Picraux, S. T. Growth, Defect Formation, and Morphology Control of Germanium-Silicon Semiconductor Nanowire Heterostructures. *Nano Lett* **2011**, *11*, 4200–4206.
50. Vaudin, M. D.; Cunningham, B.; Ast, D. G. The Structure of 2nd-Order and 3rd-Order Twin Boundaries in Silicon. *Scripta Metall Mater* **1983**, *17*, 191–198.
51. Cerva, H. High-Resolution Electron-Microscopy of Diamond Hexagonal Silicon in Low-Pressure Chemical Vapor-Deposited Polycrystalline Silicon. *J. Mater. Res.* **1991**, *6*, 2324–2336.
52. Mclarnan, T. J. The Numbers of Polytypes in Close-Packings and Related Structures. *Z. Kristallogr.* **1981**, *155*, 269–291.
53. Anastassakis, E.; Cantarero, A.; Cardona, M. Piezo-Raman Measurements and Anharmonic Parameters in Silicon and Diamond. *Phys Rev B* **1990**, *41*, 7529–7535.
54. Sui, Z. F.; Herman, I. P. Effect of Strain on Phonons in Si, Ge, and Si/Ge Heterostructures. *Phys Rev B* **1993**, *48*, 17938–17953.
55. Wang, S. Q.; Ye, H. Q. Ab Initio Elastic Constants for the Lonsdaleite Phases of C, Si and Ge. *J Phys-Condens Mat* **2003**, *15*, 5307–5314.
56. Mermoux, M.; Crisci, A.; Baillet, F.; Destefanis, V.; Rouchon, D.; Papon, A. M.; Hartmann, J. M. Strain in Epitaxial Si/SiGe Graded Buffer Structures Grown on Si(100), Si(110), and Si(111) Optically Evaluated by Polarized Raman Spectroscopy and Imaging. *J. Appl. Phys.* **2010**, *107*, 013512.
57. Yeh, C. Y.; Lu, Z. W.; Froyen, S.; Zunger, A. Zinc-Blende-Wurtzite Polytypism in Semiconductors. *Phys Rev B* **1992**, *46*, 10086–10097.
58. Chen, J. N.; Conache, G.; Pistol, M. E.; Gray, S. M.; Borgstrom, M. T.; Xu, H. X.; Xu, H. Q.; Samuelson, L.; Hakanson, U. Probing Strain in Bent Semiconductor Nanowires with Raman Spectroscopy. *Nano Lett* **2010**, *10*, 1280–1286.
59. Adu, K. W.; Xiong, Q.; Gutierrez, H. R.; Chen, G.; Eklund, P. C. Raman Scattering as a Probe of Phonon Confinement and Surface Optical Modes in Semiconducting Nanowires. *Applied Physics A-Materials Science & Processing* **2006**, *85*, 287–297.